A new approach to detect broken rotor bars in induction machines by current spectrum analysis

Gaëtan Didier, Eric Ternisien, Olivier Caspary, Hubert Razik

▶ **To cite this version:**

Gaëtan Didier, Eric Ternisien, Olivier Caspary, Hubert Razik. A new approach to detect broken rotor bars in induction machines by current spectrum analysis. Mechanical Systems and Signal Processing, 2007, 21 (2), pp.1127-1142. 10.1016/j.ymssp.2006.03.002 . hal-00115405

HAL Id: hal-00115405
https://hal.science/hal-00115405

Submitted on 6 Dec 2006

HAL is a multi-disciplinary open access archive for the deposit and dissemination of scientific research documents, whether they are published or not. The documents may come from teaching and research institutions in France or abroad, or from public or private research centers.

L'archive ouverte pluridisciplinaire **HAL**, est destinée au dépôt et à la diffusion de documents scientifiques de niveau recherche, publiés ou non, émanant des établissements d'enseignement et de recherche français ou étrangers, des laboratoires publics ou privés.

A New Approach to Detect Broken Rotor Bars in Induction Machines by Current Spectrum Analysis

G. Didier*, E. Ternisien†, O. Caspary*, and H. Razik†

Abstract

In this paper, a new technique to detect broken rotor bars in polyphase induction machines is presented. Like most techniques, we employ the Fourier Transform of one stator current to make detection. But where the other methods use the Fourier Transform modulus, we propose an alternative approach by analyzing its phase. As shown by results, the Fourier Transform phase allows to detect one broken rotor bar when the motor operates under a low load. In order to improve the diagnosis and to permit the detection of incipient broken rotor bar, we complete the analysis with the Hilbert Transform. This transform provides good results and a partially broken rotor bar can be detected when the load torque is equal or greater than 25%. The main advantage of these methods is that it does not require a healthy motor reference to take the final decision on the rotor cage state.

keywords : Phase analysis, Fourier Transform, Hilbert Transform, Fault diagnosis, Induction machines.

1 Introduction

Nowadays, no one can deny the important role of the asynchronous motor in industry applications. It is well-known that an interruption of a manufacturing process due to a mechanical or electrical problem induces a significant financial loss for the firm. Interruptions can be caused by rotor faults (broken rotor bars or cracked rotor end ring), stator faults (opening of a stator phase or inter-turn short circuits) , rotor-stator eccentricity (static and dynamic eccentricity) and bearing failures [1], [2]. In order to avoid such problems, we have to detect these faults to prevent a major failure from occurring.

Broken rotor bars rarely cause immediate failures, especially in large multi-pole (slow speed) motor. However, if there are enough broken rotor bars, the motor may not start as it may not be able to develop sufficient accelerating torque. Regardless, the presence of broken rotor bars precipitates deterioration in other components that can result in time-consuming and expensive fixes.

Various techniques have been developed to detect broken rotor bars in induction motors. We can quote vibration measurement [3], temperature measurement [4], coils to monitor the motor axial flux [5], Park's Vector currents monitoring [6], artificial intelligence based techniques [7]. However, the most popular techniques are based on the monitoring of the stator current spectrum (called Motor Current Signature Analysis) because of its non-intrusive feature [8, 9, 10, 11]. In this technique, the amplitude of the lateral bands created by the rotor fault around the supply frequency are monitored. An augmentation of these amplitudes allows dimensioning the failure's degree. Others use the instantaneous power spectrum of one stator phase to calculate a global fault index [12]. The disadvantage of all these methods is that the knowledge of the healthy motor stator current is necessary to take a decision about the rotor state.

In this paper, we propose a broken rotor bar detection method using the line current Discrete Fourier Transform (DFT) phase. This technique does not require the healthy motor current knowledge, which is a major advantage compared to the classical ones. We will show that the basically calculated phase gives good results when the motor operates near its nominal load. For weak load, the results obtained are not robust enough especially for the detection of an incipient rotor fault. This problem will be solved by using the Hilbert Transform applied to the line current spectrum modulus. Thanks to this method, the diagnosis of a partially broken rotor bar could be carried out without reference even if the motor operates at low load (25% of the rated torque).

*Groupe de Recherche en Electrotechnique et Electronique de Nancy, GREEN-CNRS UMR-7037, Université Henri Poincaré, 54506 Vandœuvre-lès-Nancy Cedex, France. e-mail: gaetan.didier@green.uhp-nancy.fr;hubert.razik@green.uhp-nancy.fr

†Centre de Recherche en Automatique de Nancy, CRAN-CNRS UMR-7039, Université Henri Poincaré, 54506 Vandœuvre-lès-Nancy Cedex, France. e-mail: eric.ternisien@iutsd.uhp-nancy.fr; olivier.caspary@iutsd.uhp-nancy.fr

2 Current monitoring

Consider an ideal three-phase supply and an asynchronous motor connected in wye. Thus the instantaneous current circulating in one phase is defined as:

$$i_{s0}(t) = \sqrt{2} I_s \sin(\omega_s t - \varphi) \tag{1}$$

with regard to the instantaneous voltage:

$$v(t) = \sqrt{2} V_s \sin(\omega_s t) \tag{2}$$

The term φ represents the phase angle between the voltage and the line current. We can see in Eq. (1) that the power spectrum of the current will contain only one fundamental component at frequency $f_s = \omega_s / 2\pi$.

When one bar breaks, a rotor asymmetry is thus created. The result is the appearance of a backward rotating field at the slip frequency sf_s (s represents the slip and f_s the supply frequency). This induces, in the stator current spectrum, an additional component at frequency $f_{bb_1}^- = (1-2s)f_s$. This cyclic current variation causes a speed oscillation at twice the slip frequency $2sf_s$ [14]. This speed oscillation induces, in the stator current spectrum, an upper component at $f_{bb_1}^+ = (1+2s)f_s$, and so on. By extension, the broken rotor bar creates additional components in the spectrum modulus at frequencies given by [14]:

$$f_{bb_k}^{\pm} = (1 \pm 2ks) f_s \qquad k = 1, 2, 3, \ldots \tag{3}$$

The effects of a broken rotor bar can be seen in Fig. 1. We represent the line current spectrum in the case of a healthy rotor in Fig. 1(a), and with one broken rotor bar in Fig. 1(b). We can see that the appearance of a rotor fault increase the amplitude of the component situated at frequencies $f_{bb_k}^{\pm}$. The amplitude of these frequencies are dependent of three factors. The first is the motor's load inertia, the second is the motor's load torque (current in the rotor bars) and the third is the severity of the rotor fault. For example, the magnitude of these components will be more important with three broken bars than with a fissured one. If we analyze Fig. 1(a), we notice that the current spectrum contains a component at the frequency $f_{bb_1}^- = (1-2s)f_s$. This frequency is created by the asymmetry existing in all induction motors and is usually used as reference for the rotor fault diagnosis.

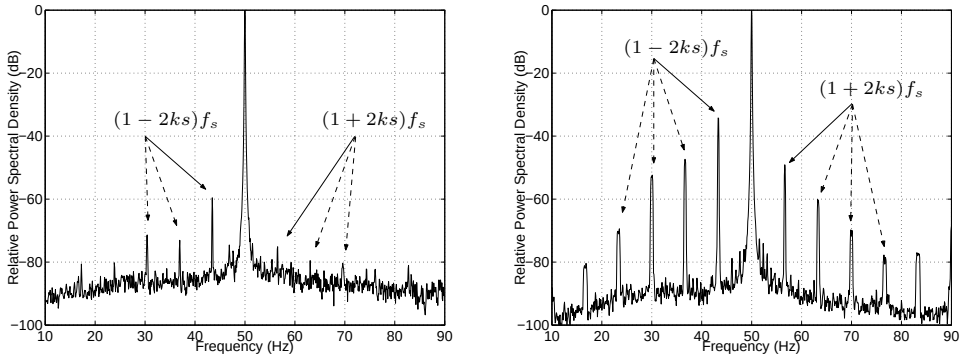

(a) Healthy rotor

(b) One broken bar

Figure 1: Line current spectrum modulus for a healthy rotor (a) and a rotor with one broken bar (b)

The classical broken bar detection methods usually use the monitoring of the line current Fourier Transform modulus. They are based on the appearance or the increase of the components amplitude at frequencies defined in Eq. (3). Appearance or increase are two terms which induce the comparison with a reference which is often the Fourier Transform modulus of the current line absorbed with a healthy rotor as we explained previously.

In this work, the spectrum reference given by the line current of the healthy motor is not necessary anymore. Thus, we propose to detect a broken rotor bar without *a priori* knowledge of the motor state.

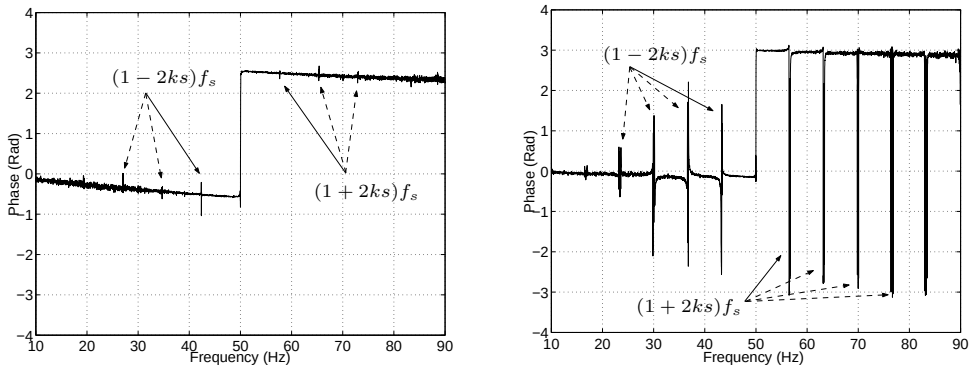

(a) Healthy rotor (b) One broken bar

Figure 2: Line current spectrum phase for a healthy rotor (a) and a rotor with one broken bar (b)

3 Discrete Fourier Transform (DFT) phase analysis

The DFT is naturally obtained by a discretisation at the sampling frequency of the Discrete Time Fourier Transform (DTFT) given by:

$$X(f) = \sum_{n=0}^{N-1} x(n) e^{-2j\pi nf} \tag{4}$$

In the case where $x(n) = e^{2j\pi nf_0}$, the DTFT of $x(n)$ is written:

$$X(f) = \sum_{n=0}^{N-1} e^{2j\pi nf_0} e^{-2j\pi nf} = \frac{\sin(N\pi(f-f_0))}{\sin(\pi(f-f_0))} e^{-j2\pi(N-1)(f-f_0)} \tag{5}$$

In this expression, we find the Dirichlet function $\frac{\sin(N\pi f)}{\sin(\pi f)}\, e^{-j2\pi(N-1)f}$ introduced by the DTFT of the rectangular window.

Let us consider the following line current expression:

$$\begin{aligned} i_s(t) &= i_{s0}(t) + \sum_{k=1}^{K_l} \frac{\sqrt{2} I_s m_{c_k}^-}{2} \cos(2\pi(f_s - k\, f_f)t - \varphi_k^-) \\ &\quad + \sum_{k=1}^{K_r} \frac{\sqrt{2} I_s m_{c_k}^+}{2} \cos(2\pi(f_s + k\, f_f)\, t - \varphi_k^+) \end{aligned} \tag{6}$$

where $m_{c_k}^-$ and $m_{c_k}^+$ represent the modulation index of the left component k and the modulation index of the right component k with regards to the supply frequency f_s in the spectrum modulus. Their values are a function of the fault level present in the rotor cage as we showed in [12]. Terms φ_k^- and φ_k^+ represent the dephasing of the component (left or right) according to the origin (0 rad). Terms K_l and K_r respectively represent the number of components at the left and at the right of the carrier frequency present in the line current spectrum for a healthy or faulty rotor. The frequency f_f represents the modulation frequency introduced by the natural asymmetry or by the rotor fault ($f_f = 2sf_s$). The corresponding line current spectra are given in Figs. 1.

Classically, the diagnosis methods use the DFT modulus of the line current defined in Eq. (6) to detect a fault. We have chosen to use the phase because it gives a better representation of the information contained in the line current. Indeed, the components at frequencies $f_{bb_k}^{\pm}$ (Eq. (3)) are present, and their amplitudes are a function of the fault level, as we can see in Figs. 2.

In fact, on each side of the 50 Hz, we observe the presence of phase jumps between $+\pi$ and $-\pi$. These phase jumps are another representation of the components present in the line current spectrum modulus. Furthermore, in this representation, we can observe a phase jump at the 50 Hz frequency.

The presence of this jump is due to the fact that the frequencies contained in the line current spectrum are not a multiple integer of the resolution frequency Δf used ($\Delta f = F_e/N$ where F_e and N respectively represent the sampling frequency and the total number of points used for the calculation of the line current spectrum).

Indeed, in the case where f_s and f_f are multiple integers of Δf ($f_s = x\,\Delta f$ and $f_f = x\,\Delta f$ with x an integer) the line current spectrum phase is illustrated in the Fig. 3(a) for $f_f = 6$ Hz (parameters used in this case are indexed in Table 1). We obtain the dephasing of all sinusoids contained in the line current expression $i_s(t)$. However, in the case where the frequencies f_s and f_f are not multiple integers of Δf, we obtain the representation given in Fig. 3(b) (by preserving the same parameters). As we can see in Fig. 3(c), if the modulation indexes increase, which means the appearance of a defect in the rotor cage, the jumps present at frequencies $(1 \pm 2ks)f_s$ increase too (in this case, parameters used are given in Table 2).

Table 1: Parameters used for Figs. 3(a) and 3(b) ($K_l = K_r = 2$).

k	1^-	1^+	2^-	2^+
m_{c_k}	0.003	0.002	0.0015	0.0005
φ_k	$-\pi/4$	$\pi/3$	$-\pi/7$	$\pi/8$

Table 2: Parameters used for the Fig. 3(c) ($K_l = K_r = 2$).

k	1^-	1^+	2^-	2^+
m_{c_k}	0.004	0.003	0.002	0.001
φ_k	$-\pi/4$	$\pi/3$	$-\pi/7$	$\pi/8$

In order to understand why the phase of the line current spectrum takes this form along the frequency axis, we propose to study a simple signal. The Discrete Time Fourier Transform (DTFT) of the line current spectrum given at Eq. (6), if we consider only its fundamental component with $\varphi = 0$ (frequency f_s), can be expressed as:

$$\begin{aligned} I_s(f) &= \sqrt{2}I_s \sum_{n=0}^{N-1} \sin(2\pi f_s t)\, e^{-2j\pi nf} \\ &= \sqrt{2}I_s \sum_{n=0}^{N-1} \frac{e^{j2\pi f_s n} - e^{-j2\pi f_s n}}{2j}\, e^{-2j\pi nf} = |I_s(f)|e^{-\Psi_{I_s}(f)} \\ &= \frac{\sqrt{2}I_s \sin(N\pi(f-f_s))}{2j\sin(\pi(f-f_s))}\, e^{-j2\pi(N-1)(f-f_s)} \\ &\quad -\frac{\sqrt{2}I_s \sin(N\pi(f+f_s))}{2j\sin(\pi(f+f_s))}\, e^{-j2\pi(N-1)(f+f_s)} \end{aligned} \tag{7}$$

In this expression, we find two Dirichlet functions positioned at frequencies $-f_s$ and $+f_s$. As said previously, the DFT is a sampling of the DTFT. So, in the case where f_s is not a multiple integer of Δf, we do not find a simple component at frequency f_s in the line current spectrum modulus but parasitic undulations as shown in Fig. 4(a). Indeed, instead of sampling the DTFT when it equals 0 (case $f_s = x\,\Delta f$), the values obtained are the values of the Dirichlet functions.

The same phenomenon occurs for the real and imaginary parts of the spectrum $I_s(f)$. They are not null and depend on values taken by the real and imaginary parts of the DTFT of the line current (Fig. 4(b)).

As the phase of the DFT $\Psi_{FT}(f)$ varies according to the sign of the real and imaginary parts of $I_s(f)$ (Eq. (8)), we obtain the form given in Fig. 4(c) with a positive jump at the frequency f_s like in Figs. 2(a) and 2(b). In the ideal case, we would have obtained a component of value $-\pi/2$ located at the frequency f_s like in Fig. 3(a).

$$\Psi_{FT}(f) = \arctan\left(\frac{\mathcal{I}_{FT}(I(f))}{\mathcal{R}_{FT}(I(f))}\right) \tag{8}$$

Nevertheless, the phase jump at 50 Hz is very advantageous for the fault detection because we are no longer disturbed by the fundamental component energy problem present in the spectrum modulus. This is interesting for the study of high power motors which have a weak slip (for example, the slip of a 2MW induction motor is near to 0.3%, which gives a frequency f_f of 0.3 Hz if the fundamental frequency f_s is equal to 50 Hz).

Now, let us consider the particular frequency $(1-2s)f_s$. This frequency, in the case of a healthy rotor, corresponds to the natural rotor eccentricity. So, as shown in Fig. 2(a), there is no phase jump at frequency

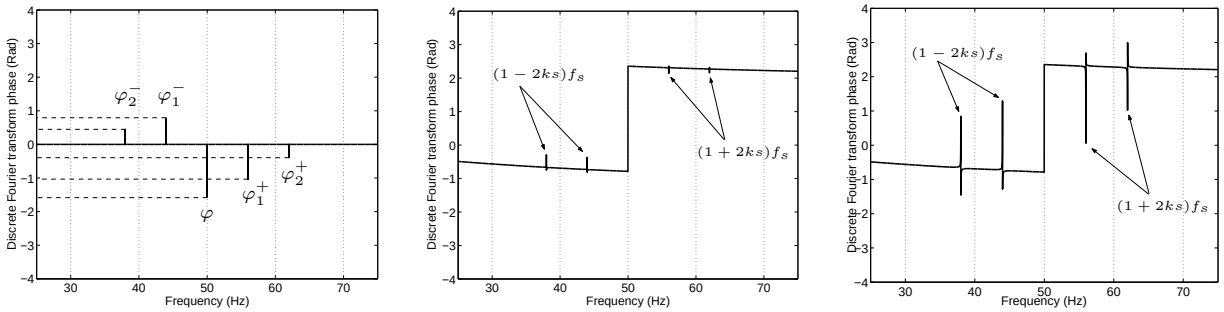

(a) $f_s = x\,\Delta f$ and $f_f = x\,\Delta f$ (b) $f_s \neq x\,\Delta f$ and $f_f \neq x\,\Delta f$ (c) $f_s \neq x\,\Delta f$ and $f_f \neq x\,\Delta f$

Figure 3: Current spectrum phase of Eq. (6): Parameters of Table 1 (a) and (b) and Parameters of Table 2 (c).

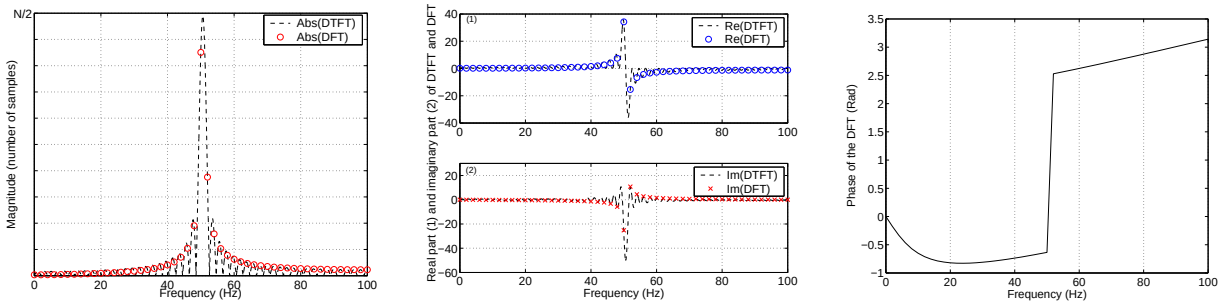

(a) Modulus of $I_s(f)$ (b) Real and imaginary parts of $I_s(f)$ (c) Phase of $I_s(f)$

Figure 4: Discrete Fourier Transform of line current (Eq. (7)) with $f_s \neq x\,\frac{F_e}{N}$.

$(1+2s)f_s$ because there is no broken rotor bar (in fact a component exists but it is masked by the noise). That is checked for all load levels studied. On the opposite, when a broken bar is present in the rotor cage (Fig. 2(b)), we can see that the phase jump at frequency $(1+2s)f_s$ is present (like the other components at frequencies given by Eq. (3)).
A simple criterion can be deduced from this observation:

- if there is no phase jump at the frequency $(1+2s)f_s$, there is **no default**;
- if there is a phase jump at the frequency $(1+2s)f_s$, there is **default**.

In order to make a more robust detection and to limit the detection of false alarms, a threshold α has been introduced in the criterion. This threshold compares the variance σ_c of $\Psi_{FT}(f)$ in the interval $B_c = [(1+2s)f_s - \frac{\delta}{2}, (1+2s)f_s + \frac{\delta}{2}]$ where the fault component is located, with the variance σ_n of $\Psi_{FT}(f)$ in the interval $B_n = [(1+2s)f_s + \frac{\delta}{2}, (1+4s)f_s - \frac{\delta}{2}]$ which contains noise. The term δ represents the frequency band width used for the calculus of σ_c (Fig. 5).
So the criterion can be reformulated as:

$$\begin{cases} \text{if} \quad \dfrac{\sigma_c}{\sigma_n} > \alpha \quad \Rightarrow \quad \text{Default} \\ \\ \text{if} \quad \dfrac{\sigma_c}{\sigma_n} \leq \alpha \quad \Rightarrow \quad \text{No Default} \end{cases} \tag{9}$$

Since the detection is based on the appearance of a significant phase jump at the frequency $(1+2s)f_s$, the first step of the algorithm is to estimate the slip of the induction motor. To do that, we recommend to use the component at frequency $(1-2s)f_s$ because, in the case of a healthy rotor, only this component is detectable. Moreover, the detection is easier at the left of the 50 Hz due to the greatest amplitude of components. Therefore, the proposed algorithm for the broken bars detection is:

1. Detection of the maxima (or minima, it depends on the phase shape) at the left of the 50 Hz;

2. Selection of the 50 Hz nearest maximum ($(1-2s)f_s$ component);
3. Computation of σ_c and σ_n with respect to the $(1+2s)f_s$ component;
4. Decision.

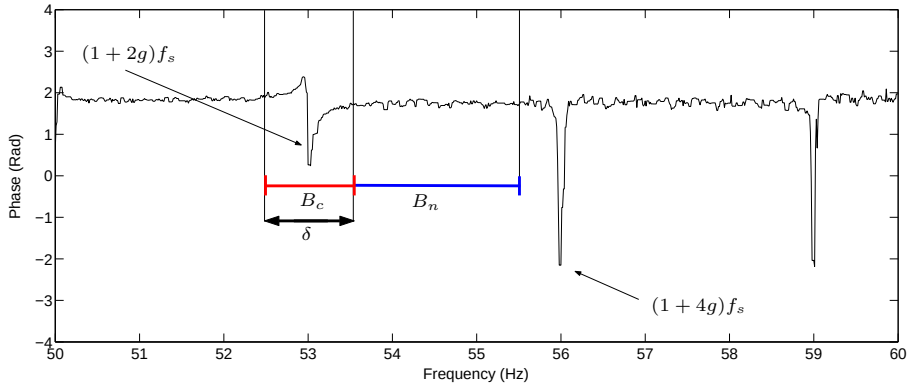

Figure 5: Variance calculus intervals on the line current spectrum phase in the frequency band [50 - 60] Hz

In fact, we can limit the frequency band used for the maxima research between $[F_0, 50]$ Hz. The frequency F_0 depends on the maximum slip of the induction motor (at full load). For our motor, the rotation speed at full load is $\Omega = 2804$rpm, so $s = 6.53\%$ and $2sf_s = 6.53$ Hz. Consequently, we choose $F_0 = 40$ Hz.

Let us note that in order to suppress the little peaks in the signal, a median filter is used. This filter has a smoother effect which helps the detection of maxima (or minima). The results of this method are presented in section 5.

To ensure the robustness of the method explained before, and to detect more precisely the incipient rotor faults, we propose another approach to improve the broken rotor bar diagnosis.

4 Hilbert Transform (HT) phase analysis

As explained in the previous section, the DFT phase, although the method gives good results, has two disadvantages. The first is that noise level is important, which makes the maxima detection and the peaks discrimination at the right of the 50 Hz (at low load) difficult. The second is that the shape of the phase is not fixed (see Figs. 8 et 10). Indeed, in the case where studied frequencies are different from Δf, the real and imaginary parts can take random values. In order to stabilize the phase shape, we must find a solution to control the real and imaginary part values of the DFT spectrum. In fact, the idea is to obtain a phase always equal to $-\pi/2$ at the left of f_s and equal to $\pi/2$ at the right of f_s, with no variation excepted at the broken bar frequencies. In other words, the real part must be null excepted at frequencies $f_{bb_k}^{\pm}$ and f_s.

The solution is to interpret the Discrete Fourier Transform modulus as the real part of a new signal called "analytic signal". Indeed, as we can see in Fig. 6(a), the modulus contains very weak values and dirac impulsions at studied frequencies. So, the shape of the real part is well-known at each frequency point and the Signal Noise Ratio (SNR) is increased.

The analytic signal is obtained by a Hilbert Transform of the line current spectrum modulus. If we consider a time signal $s(t)$, the analytic signal $\tilde{s}(t)$ can be expressed as:

$$\tilde{s}(t) = s(t) + j\rho(t). \tag{10}$$

where

$$\rho(t) = \mathcal{H}(s(t)) = s(t) * \frac{1}{\pi t} \tag{11}$$

The HT $\mathcal{H}(s(t))$ is defined as the convolution product of the signal $s(t)$ (which becomes the real part of $\tilde{s}(t)$) by a filter whose the impulse response is $h(t) = \frac{1}{\pi t}$. The analytic signal $\tilde{s}(t)$ is calculated by using different

methods [13]. One of these methods is the use of the Fourier Transform. Indeed, the Fourier Transform of the signal $\rho(t)$, which represents the Hilbert Transform of the signal $s(t)$, is given by the following equation:

$$\rho(t) \xrightarrow{\mathcal{F}} -jsgn(f)S(f) \tag{12}$$

where the function $sgn(f)$ and $S(f)$ represent respectively the signum function (distribution) given by Eq. (13) and the Fourier Transform of $s(t)$.

$$sgn(f) = \begin{cases} +1 & \text{for} \quad f > 0 \\ 0 & \text{for} \quad f = 0 \\ -1 & \text{for} \quad f < 0 \end{cases} \tag{13}$$

Consequently, the analytic signal $\tilde{s}(t)$ can be obtained by using the Fourier Transform with the expression:

$$\tilde{s}(t) \xrightarrow{\mathcal{F}} S(f) + j[-j\, sgn(f)]S(f) = [1 + sgn(f)]S(f) = x(f)S(f) \tag{14}$$

with

$$x(f) = [1 + sgn(f)] = \begin{cases} 2 & \text{for} \quad f > 0 \\ 1 & \text{for} \quad f = 0 \\ 0 & \text{for} \quad f < 0 \end{cases} \tag{15}$$

The Fourier image of the analytic signal is doubled at positive frequencies and cancelled at negative frequencies with respect to $S(f)$. The advantage of this transformation is that the result remains in the same domain as the signal analyzed (time for example). The particularity of this paper is that we do not apply the HT on the time signal $i_s(t)$ but on its spectrum modulus $|I_s(f)|$. Hence, the analytic signal of this modulus provides:

$$\widetilde{I}_s(f) = |I_s(f)| + j\, I_{HT}(f) \tag{16}$$

with

$$I_{HT}(f) = \mathcal{H}(|I_s(f)|) \tag{17}$$

We represent in Eq. (18) the diagram used to obtain the analytic signal $\widetilde{I}_s(f)$ with the Fourier Transform.

$$\begin{array}{ccc} |I_s(f)| & \xrightarrow{\mathcal{F}} & S(z) \\ \uparrow{\scriptstyle \mathcal{R}(\widetilde{I}_s(f))} & & \downarrow{\scriptstyle .\, x(z)} \\ \widetilde{I}_s(f) & \xleftarrow{\mathcal{F}^{-1}} & x(z)S(z) \\ \downarrow{\scriptstyle \mathcal{I}(\widetilde{I}_s(f))} & & \\ I_{HT}(f) & & \end{array} \tag{18}$$

The analytic signal phase $\Psi_{HT}(f)$ can be calculated with the expression:

$$\Psi_{HT}(f) = \arctan\left(\frac{\mathcal{I}(\widetilde{I}_s(f))}{\mathcal{R}(\widetilde{I}_s(f))}\right) = \arctan\left(\frac{I_{HT}(f)}{|I_s(f)|}\right) \tag{19}$$

The real part $|I_s(f)|$, the imaginary part $I_{HT}(f)$ and the phase $\Psi_{HT}(f)$ of the analytic signal are shown in Figs. 6 in case of one broken rotor bar.

In conclusion, the Hilbert Transform applied to the spectrum modulus gives a phase restricted to the interval $\left[-\frac{\pi}{2}, \frac{\pi}{2}\right]$. Moreover, the knowledge of the imaginary part form Eq. (11) allows to predict the exact form of the analytic signal phase.

Thanks to the noise reduction, the phase jumps are more pronounced which permits an easier detection. The noise level is lower than in $\Psi_{FT}(f)$ because of the redefinition of $|I_s(f)|$ and $I_{HT}(f)$ thanks to the Hilbert Transform. The algorithm is the same as for the DFT phase detection.

5 Experimental results

The test-bed used in the experimental investigation is composed of one three phase induction motor, 50 Hz, 2-poles, 3kW. In order to test the effectiveness of the suggested methods, several identical rotors can be exchanged without affecting the electrical and magnetic features. The squirrel cage has 28 rotor bars (Figs. 7). The voltage

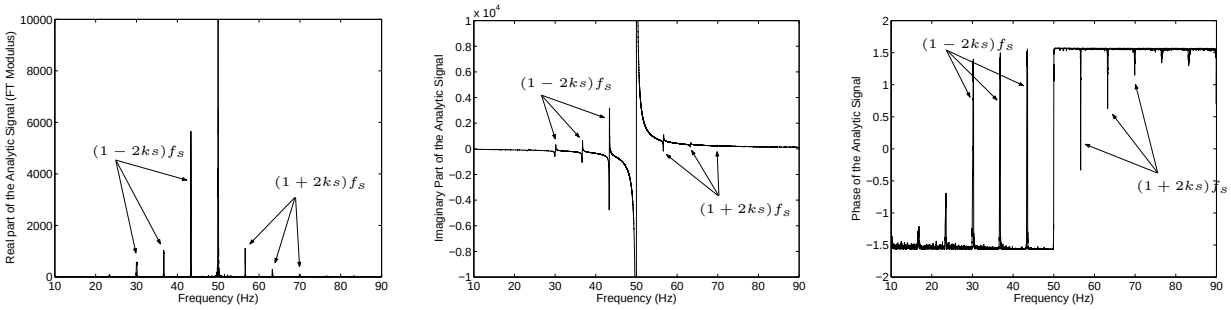

(a) (b) (c)

Figure 6: Real part (a), imaginary part (b) and phase (c) of the analytic signal $\tilde{I}_s(t)$ (for one broken rotor bar).

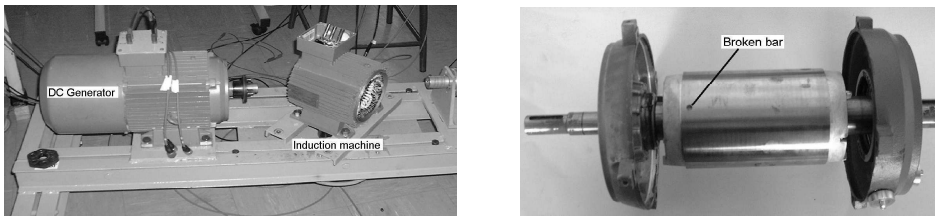

(a) (b)

Figure 7: Test-bed and rotor with one broken bar

and the line current measurements were made at the nominal rate. For those two variables, the sampling frequency F_e was 2k Hz and each data length was equal to 2^{18} values. We decided to study the case of a partially broken rotor bar (approximately 50% of the bar is bored) and one broken rotor bar. Indeed, the detection of an incipient rotor fault remains, nowadays, still difficult.

The results obtained using the Discrete Fourier Transform phase are given in Table 3 (for example we note H-L100 the case of a healthy rotor with 100% load and 05b-L25 the case of a partially broken rotor bar with 25% load). We represent in Figs. 8 and 10 the DFT phase when the torque applied to the machine is equal to 100% and 25% of the rated torque.

We chose to take α equal to 3. This value was selected according to the experimental results carried out. The analysis of the results shows us that the detection of one broken rotor bar is possible at a load torque higher than 25%. On the other hand, the detection of an incipient rotor defect (a partially broken rotor bar) can be made only if the load torque applied to the machine is at least equal to 50%.

This non-detection is mainly due to the important noise present in the phase signal. Indeed, we can notice that noise increases when the load applied to the machine decreases (Figs. 10(a), 10(b) and 10(c) in comparison with Figs. 8(a), 8(b) and 8(c)). For these operating modes, the variance σ_n is important, which makes the detection of the rotor defect more difficult because the ratio σ_c/σ_n is too weak so that the algorithm of decision considers that the rotor cage does not present a defect.

When the asynchronous machine operates with no load, the algorithm of detection does not take any decision. That means that the jump located at the frequency $(1-2s)f_s$ is not detectable due to its low amplitude. The current which crosses the rotor bars is not important enough to create a consequent jump at this frequency. Thus, the algorithm cannot evaluate the slip of the asynchronous machine and so the two frequency bands B_c and B_n.

If we consider that an asynchronous machine operates most of its time at its rated torque, we can be satisfied with the results given by the analyses of the Discrete Fourier Transform phase.

We show in Table 4 the results obtained with the analytical signal phase. For these analysis, we chose the α coefficient equal to 10. This value is different for the two methods because the SNR of the Hilbert Transform phase is greater than the DFT phase one.

We can note that the two rotor defects (a broken bar and a partially broken bar) are detected when the load torque is contained between 25% and 100% of the rated torque. The non-detection of the jump at frequency

$(1-2s)f_s$ is always present when the machine is unloaded.

If we do not consider this particular case, we thus obtain better results compared to those given in Table 3. This better detection is due to the fact that noise contained in the analytical signal phase is far less important when the machine operates under low load torque. Figs. 11(a), 11(b) and 11(c) illustrate the use of Hilbert Transform applied to the line current spectrum modulus compared to the Figs. 10(a), 10(b) and 10(c). The weak noise contained in the frequency band $[(1+2s)f_s + \frac{\delta}{2}, (1+4s)f_s - \frac{\delta}{2}]$ gives a more sensitive detection algorithm in case on incipient rotor defect. Indeed, in this case, the calculation of variances σ_c and σ_n is more optimal than the previous method. Furthermore, it is obvious that the maxima are more easily detectable as we can see in Figs. 9 and 11.

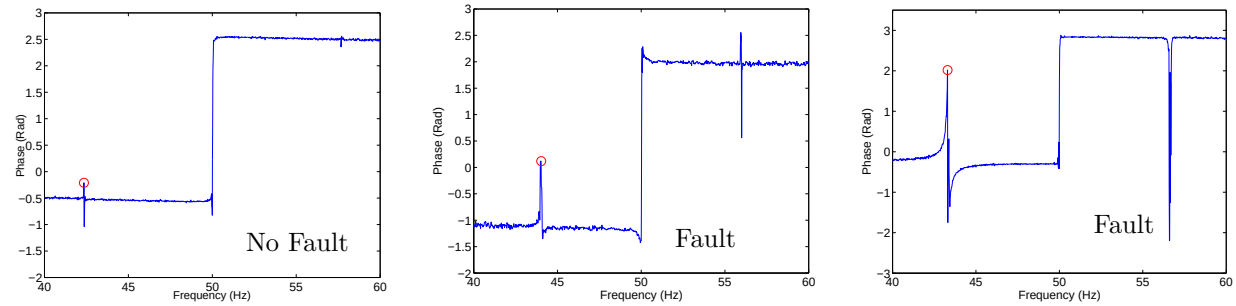

(a) Healthy rotor (b) Half-broken rotor bar (c) One broken bar

Figure 8: Fault detection with the line current spectrum phase analysis under 100% load.

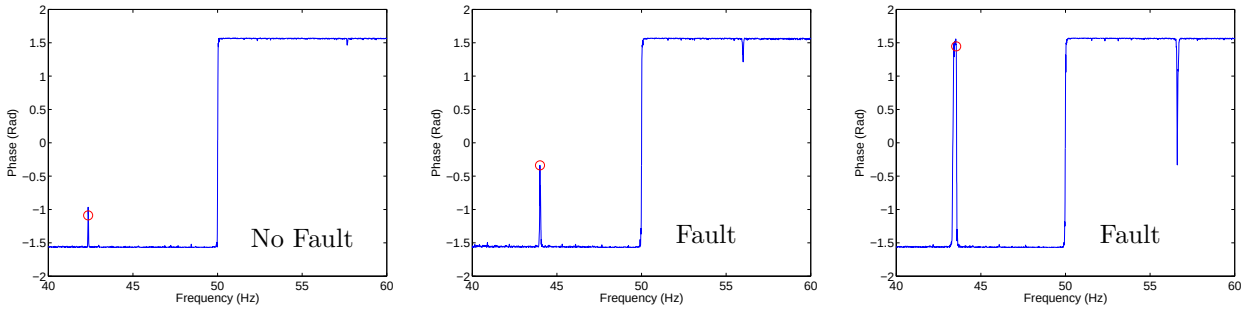

(a) Healthy rotor (b) Half-broken rotor bar (c) One broken bar

Figure 9: Fault detection with the analytic signal phase analysis under 100% load.

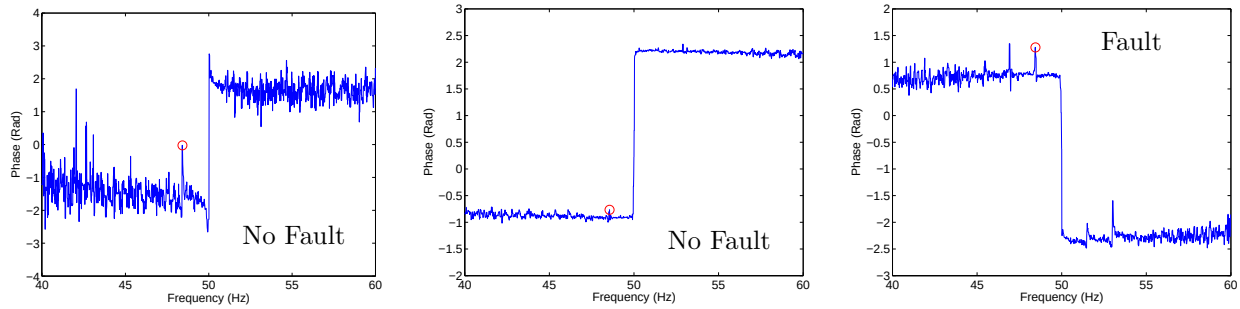

(a) Healthy rotor (b) Half-broken rotor bar (c) One broken bar

Figure 10: Fault detection with the line current spectrum phase analysis under 25% load.

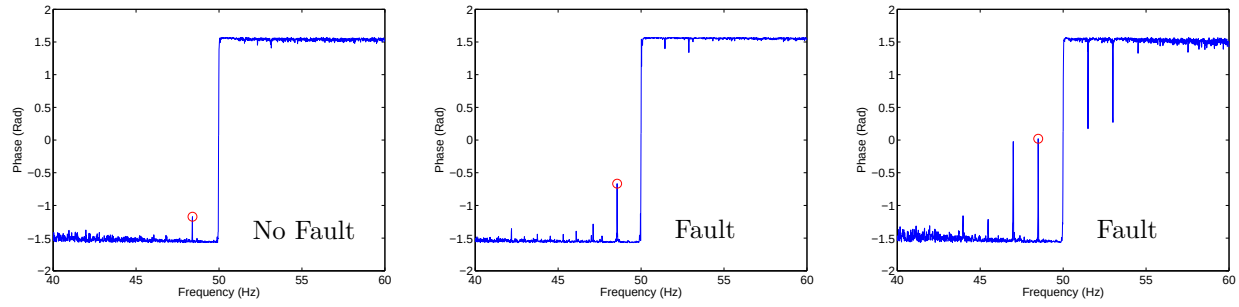

(a) Healthy rotor (b) Half-broken rotor bar (c) One broken bar

Figure 11: Fault detection with the analytic signal phase analysis under 25% load.

Table 3: Fault detection by DFT phase analysis

Rotor state	$(1-2s)f_s$ **frequency**	σ_c	σ_n	$\frac{\sigma_c}{\sigma_n}$	**No Default**	**Default**
H-L100	43.49	0.0037	0.0067	0.5525	X	
05b-L100	44.03	0.0147	0.0008	19.4797		X
1b-L100	43.28	2.6171	0.0002	14500		X
H-L75	45.08	0.0033	0.0034	0.9743	X	
05b-L75	45.74	0.3637	0.0001	2500		X
1b-L75	45.45	0.1827	0.0049	37.4356		X
H-L50	No max detection				No decision	
05b-L50	47.13	0.0004	0.0002	2.6286	X	
1b-L50	46.97	0.2113	0.0030	70.4681		X
H-L25	48.42	0.0712	0.0574	1.2412	X	
05b-L25	48,57	0.0004	0.0003	1.1345	X	
1b-L25	48.45	0.0043	0.0006	7.1024		X
H-L0	No max detection				No decision	
05b-L0	No max detection				No decision	
1b-L0	No max detection				No decision	

Table 4: Fault detection by analytic signal phase analysis

Rotor state	$(1-2s)f_s$ **frequency**	σ_c	σ_n	$\frac{\sigma_c}{\sigma_n}$	**No Default**	**Default**
H-L100	43.45	0.0003	5.31E-05	5.3785	X	
05b-L100	44.00	0.0038	4.49E-05	84.0466		X
1b-L100	43.54	0.1103	2.51E-05	4390		X
H-L75	45.08	0.0003	5.13E-05	6.2159	X	
05b-L75	45.70	0.0028	5.04E-05	54.6524		X
1b-L75	45.45	0.1103	3.56E-05	3100		X
H-L50	46.79	0.0004	8.86E-05	4.4387	X	
05b-L50	47.14	0.0014	3.66E-05	38.1296		X
1b-L50	47.01	0.0748	12.9E-05	578.6473		X
H-L25	48.40	0.0002	36.9E-05	0.6299	X	
05b-L25	48.56	0.0005	3.50E-05	14.2723		X
1b-L25	48.50	0.0239	35.7E-05	66.966		X
H-L0	No max detection				No decision	
05b-L0	No max detection				No decision	
1b-L0	No max detection				No decision	

The key point is that both techniques work with any knowledge of healthy rotor. But for an acceptable response, the load must be at least 25% in order to have a minimum current in the rotor to make the phase jump at $(1-2s)f_s$ distingable.

In case of limited number of samples (for example 4096 samples), the broken rotor bar can still be detected by the analytic signal phase method. By contrast, the Discrete Fourier Transform method provides bad results since the fault is not detected. This is due to the deficient resolution induced by the reduction of the sample number. The HT method is insensitive to this variation thanks to its principle, but a reduction of the phase jumps amplitude is visible. Consequently, we can conclude that a minimal number of samples is required to make a good detection. For example, in our case, the detection of one broken rotor bar for a full load operation is possible with 4096 samples, but at 50% load, 8192 samples are needed to make rotor fault detection.

6 Conclusion

The proposed methods in this article are based on the analysis of the line current spectrum. We showed that information contained in the spectrum modulus (components at frequencies $(1 \pm 2ks)f_s$) is also visible in the DFT phase at the same frequencies, in the form of phase jumps. Indeed, these phase jumps also depend on the presence or the absence of broken bars in the rotor cage. The results obtained with the DFT phase are satisfying in case of one broken rotor bar, but the importance of the noise level prevents the detection of a partially broken rotor bar. In order to reduce the noise in the phase signal and to make the detection more reliable, a second method is put forward. This one uses the modulus of the line current Discrete Fourier Transform as the real part of a new complex signal obtained by the Hilbert Transform. This method provides better results since we detect a partially broken rotor bar for a load level equals to 25%. Besides, the Hilbert Transform method is less sensible to number of samples variation than the DFT. This property could make easier the implantation on a DSP.

The essential point described in this article is the detection without *a priori* knowledge of the healthy motor. It is distinguished from the traditional methods which need this reference.

7 Acknowledgment

The authors wish to express their gratefulness to the Research Ministry and to H. Poincaré University for their financial support in the development of the test-bed.

References

[1] A.H. Bonnet, Analysis of Rotor Failures in Squirrel Cage Induction Machines, IEEE Transactions on Industry Applications 24 (6) (1988) 1124–1130.

[2] A.H. Bonnet and G.C. Soukup, Cause and Analysis of Stator and Rotor Failures in Three-Phase Squirrel-Cage Induction Motors, IEEE Transactions on Industry Applications 28 (4) (1992) 921–937.

[3] S. Pöyhönen, P. Jover and H. Hyötyniemi, Independent Component Analysis of Vibrations for Fault Diagnosis of an Induction Motor, Proceedings of the IASTED International Conference Circuits, Signals and Systems, Mexico, May 2003, Vol. 1, pp. 203-208.

[4] H. Yahoui and G. Grellet, Measurement of physical signals in the rotating part of an electrical machine by means of optical fibre transmission, ARTICLE Measurement 20 (3) (1997) 143–148.

[5] G.B. Kliman, R.A. Koegl, S. Stein, R.D. Endicott and M.W. Madden, Noninvasive detection of broken rotor bars in operating induction motors, IEEE Transactions on Energy Conversion EC-3 (4) (1988) 873–879.

[6] M. E. H. Benbouzid, A review of induction motors signature analysis as a medium for faults detection, IEEE Transactions on Industrial Electronics 47 (5) (2000) 984–993.

[7] F. Filippetti, G. Franceschini, C. Tassoni and P. Vas, Recent developments of induction motor drives fault diagnosis using AI techniques, IEEE Transactions on Industrial Electronics 47 (5) (2000) 994–1004.

[8] W.T. Thomson and M. Fenger, Current Signature Analysis to Detect Induction Motor Faults, IEEE Transactions on IAS Magazine 7 (4) (2001)26–34.

[9] G.B. Kliman and J. Stein, Induction motor fault detection via passive current monitoring, International Conference on Electrical Machines 1 (1990) 13–17.

[10] R. Fiser and S. Ferkolj, Detecting Side-band Frequency Components in Stator Current Spectrum on Induction Motor for Diagnosis Purpose, Automatika, Journal for Control, Measurement, Electronics, Computing and Communications 40 (3-4) (1999) 155–160.

[11] G. Didier, H. Razik and A. Rezzoug, On the Modelling of Induction Motor Including the First Space Harmonics for Diagnosis Purposes, International Conference on Electrical Machine, CD-ROM, August 2002.

[12] G. Didier, H. Razik, O. Caspary and E. Ternisien, Rotor Cage Fault Detection in Induction Motor using global modulation index on the Instantaneous Power Spectrum, Symposium on Diagnostics, Electric Machines, Power Electronics and Drives, August 2003.

[13] A.D. Poularikas, *The Transforms and Applications Handbook, Second Edition*. CRC Press.

[14] F. Filipetti, G. Franceschini, C. Tassoni and P. Vas, Impact of speed ripple on rotor faukt diagnosis of induction machine, International Conference on Electrical Machines, Vol. 2, 1996, pp. 452–457.